Materials Research. 2022; 25:e20210449
DOI: https://doi.org/10.1590/1980-5373-MR-2021-0449

The role of Preparation Technique on the Structure, Electrical Properties of $Co_xZn_{1-x}Fe_2O_4$ and its Electrocatalytic Effect on Hydrogen Evolution Reaction

A.M. Fathi[a], *R.M. Khattab*[b], *H.E.H.Sadek*[b], *A.H.Salama*[a]

[a]*National Research Centre, Physical chemistry department, Dokki, 12622, Cairo, Egypt.*
[b]*National Research Centre, Refractories, Ceramics and Building Materials Department, Dokki, 12622, Cairo, Egypt.*

Received: September 6, 2021; Revised: February 4, 2022; Accepted: March 13, 2022.

Zinc-ferrite $ZnFe_2O_4$ and $Co_xZn_{1-x}Fe_2O_4$ (x= 0.2, 0.5 and 0.8) were prepared by two different techniques. The first was the solid state reaction based on utilizing electric arc furnace dust (waste material), and the second was the microwave treatment (pure materials). The structure and characterization of the prepared samples were studied by using XRD and SEM which ensured the formation of cubic spinel structure with some hematite phases. The physical properties as the density and porosity were measured where the microwave samples showed lower porosity and higher density than the solid state samples. Semiconducting properties has been observed for the prepared samples. The electrocatalytic activity of the hydrogen evolution reaction (HER) has been studied for all the samples in 1.0 M KOH (25 °C) by cyclic voltammetry, linear sweep voltammetry, and electrochemical impedance techniques. The results showed that the catalytic activity increased with increase of Co content as the surface area and the total pore volume increases in the ferrite prepared by solid state method while $Co_{0.2}Zn_{0.8}Fe_2O_4$ prepared by microwave method showed the highest surface area and optimum improvement in the apparent HER catalytic activity. Lower resistance and faster charge transfer were shown for $Co_xZn_{1-x}Fe_2O_4$ than the pure phase.

Keywords: *Spinel, Feritte, microwave, electrocatalyst, HER.*

1. Introduction

A lot of interest was attained for spinel ferrite due to their unique properties as the catalytic properties, magnetic, dielectric, thermal and electrical conductivity[1-3]. Zinc ferrite is a normal spinel structure, all of the A(Zn^{2+}) sites are tetrahedral coordinated while the B(Fe^{3+}) sites are octahedral coordinated by oxygen atoms. Synthesis and applications of nanoparticles of spinel structured ferrite (AB_2O_4) are amid the most important research topics due to their remarkable chemical, physical and magnetic properties. The probability of preparing ferrites in the form of nanoparticles has opened a new and exciting research field, with revolutionary applications not only in the electronic technology but also in the field of biotechnology. Several techniques have been developed for the synthesis of such nanoparticle such as sol-gel, hydrothermal, co-precipitation, aerosol, etc[4-7].

Among the various methods reported in literature, microwave combustion technique is the most effective and feasible route for the rapid synthesis of nanomaterials with high homogeneity, purity and improved characteristics. Unlike conventional heating method, microwave energy is an internal means of heat energy generation and conversion. The microwave energy is transformed into heat energy by strong inter-molecular friction and rises the temperature of the precursor materials suddenly[8]. Conventional sintering method is usually used for the preparation of Ferrite with a slow heating rate where the process takes long time and coarsening in the microstructure occurs. The microwave sintering method can avoid these problems[9] and produces materials with attractive properties[10,11]. As a result, the morphology, surface area, crystallite size, textural, and other physicochemical properties are largely altered. Also, the use of microwave energy as heating source speeds up the chemical reaction and kinetics, which reduces energy loss and improves the economic viability[12,13].

Electric arc furnace (EAF) dust is a complex material generated during the steel making process varies essentially from one steel production unit to another by their morphological and chemical composition to a significant extent[14-19]. The EAF dust is rich in oxides and in many cases contains heavy metals such as cadmium, lead, zinc and chromium[14,16]. Due to the presence of these heavy metals, the steel dust is considered as an industrial toxic waste and is listed as a K061 hazardous industrial solid waste by the Environmental Protection Agency (EPA) in United States and tabulated as a hazardous material with the code 100213 in European Union waste catalogue[16]. Depending on the type of steel produced, it composed mainly of Fe and Zn in addition to variable amounts of Ca, Pb, Ni, Cd, Co, etc. Moreover, the most content of zinc in EAF dust comes from the scrap coatings[15-18,20,21]. Nearly, 15–20 kg of the EAF dust is formed as a by-product per one ton of steel produced through the EAF[15-19,21]. There are three suggested ways for dealing with the EAF dust: firstly, recycling the EAF dust back into the EAF[22], secondly treating the EAF dust at a certain temperature for extraction of zinc and other valuable

*e-mail: amfathi70@yahoo.com

metals[18-20,23], such as iron[20], lead[23], and finally processing the EAF dust by stabilization for landfill disposal. The structural and electrical properties of ferrites are sensitive to preparation method, sintering temperature, sintering time, rate of heating and rate of cooling[24,25]. The study of electrical resistivity produces valuable information on behaviour of free and localized electric charge carried in the sample.

The spinel structure allows the doping of different metal ions without altering the spinel structure and modifying electrical structural, dielectric, or magnetic properties of spinel ferrites via substituting M^{+2} ions[9-11,26] due to the modification of the distribution of the ions in the spinel assembly. The concentration of third metal ion alters the distribution of Fe^{+3} and M^{+2} ions affecting the magnetic, catalytic, and electrical or dielectric properties[27,28].

In recent years, different materials was used to catalyse the water splitting in both acidic and alkaline media[29-32], However spinel oxides have attracted an interest in catalysing the oxygen evolution reaction (OER) due to their efficiency and cost-effectiveness[2,33,34]. Nowadays, finding low cost electrode materials with good electrical and kinetic properties was the main aim. Thus, in this paper, we will focus more light on using EAF waste to prepare useful materials $Co_XZn_{1-X}Fe_2O_4$ with different Co concentrations 0.2, 0.5 and 0.8) which can be used as electrocatalyst for water electrolysis. The effect of the preparation technique, sintering temperature and Co concentration on the structure, characterization, and electrical properties of the prepared spinel has been be studied and tested as an electrocatalyst for hydrogen evolution reaction (HER) and oxygen evolution reaction (OER).

2. Experimental Methods

2.1. Starting materials

The EAF dust was supplied by Ezz Flat Steel Company. Suez, Egypt. XRF analysis of the representative dust was determined in Table 1. Highly pure chemical materials Zinc acetate (99,9%) and hydrate ferric chloride ($FeCl_3$. $6H_2O$, 99.9%) were supplied by Fluka and Alpha, respectively. Zinc oxide (ZnO) was supplied by VEB (Germany) and cobalt oxide Co_3O_4 was supplied by (SRL, India). Cobalt(II)-cholride hexhydrate was supplied by AppliChem.

Table 1. XRF of the EAFD dust.

Oxide	Wt.-%
SiO_2	3.03
TiO_2	0.07
Al_2O_3	0.45
Fe_2O_3	46.69
ZnO	9.10
CaO	11.08
K_2O	1.81
Na_2O	8.10
P_2O_5	0.17
SO_3	2.32
MgO	2.92
Br	0.08
Cl	2.50
L.O.I	8.59

2.2. Samples preparation

2.2.1. For batches prepared by microwave combustion method

Firstly, four spinel compositions of $Co_xZn_{1-x}Fe_2O_4$ (0, 0.2, 0.5 and 0.8 Co contents and designed as Co0, Co0.2, Co0.5 and Co0.8) were prepared with stoichiometric ratios using urea as a fuel. The starting materials used for preparing this composition are Zinc acetate, hydrate ferric chloride and cobalt chloride hexahydrate. Millipore water was used as solvent during sample preparation processes. The compounds were dissolved separately in Millipore water and mixed together in a glass beaker at room temperature for about 1 h to obtain a homogeneous solution. While urea was served as a fuel, the inorganic materials in the precursors were the oxidizers in the combustion method. The fuel to oxidizer ratio (F/O) was equal to 1:1 M ratio. Then pouring the homogeneous solutions into a silica crucible and placed inside the microwave-oven for irradiation. Then subject the crucible to power 1000 W for 10 min at temperature 300 °C and frequency 2.45 GHz. Initially, the solution boiled and underwent dehydration followed by decomposition with the evolution of gases. After that these powders were calcined at 800 °C; then pelletized (1 cm x 1 cm) and sintered at temperatures; 1400°C.

2.2.2. For batches prepared by solid state reaction based on utilizing electric arc furnace dust

Four batches were prepared based on utilizing electric arc furnace dust, ZnO and Fe_2O_3 oxides to prepare the spinel $Co_xZn_{1-x}Fe_2O_4$ structure (0, 0.2, 0.5 and 0.8 Co contents). The powders were well mixed and uniaxially semi-dry pressed at 50 MPa in a disc shape mold having ½ inch diameter and height. The pressed specimens were then sintered at 800, 850, 900°C for 2 h in an electric furnace to follow the phase composition.

2.3. Characterization

The bulk density and apparent porosity of the fired samples were determined by Archimedes method. To investigate the phase composition, a computer-interface X-ray diffractometer (XRD) (Bruker D8 diffractrometer) using nickel-filtered CuKα radiation was used.

Scanning electron microscopy (SEM) was applied to determine the morphological nature of the prepared samples. The SEM measurement device was a high-resolution Quanta field-emission gun (FEG) 250 (FEI company) attached to an EDAX unit to perform elemental analysis using an accelerating voltage of 30 kV, a magnification from 10x up to 400,000x, and a wavelength resolution of 3.5 nm.

The surface area and porosity were determined from nitrogen adsorption isotherms measured at 77 K with NOVA 2200 Gas Sorption Analyzer (Quantachrome). Prior to the measurements, the sample was outgassed overnight at 300 °C. The specific surface area (SBET) was estimated by Brunauer- Emmett- Teller (BET) equation. The amount of nitrogen adsorbed at the relative pressure of p/p0 = 0.96 was employed to determine the total pore volume (VT). The micropore volume (VDR) was calculated by applying the Dubinin-Radushkevich equation. The mesopore volume

(Vmes) was calculated as a difference between VT and VDR. The pore size distributions were determined by means of the Quenched Solid Density Functional Theory (QSDFT).

2.4. Electrical studies

The conductivity of the prepared samples was measured using an LCR Hi Tester (HIOKI, 3532-50) on a frequency range of 42 Hz to 1 MHz with a 0.1 V applied voltage in the temperature range 25–250 °C. The samples have been performed in the form of pellets of about 10 mm in diameter, and thickness ranged from 0.51 to 1.07 mm, which was prepared by pressing powdered samples at 10 ton /cm^2.

The real part of the dielectric function (constant) ε` of the samples was calculated from the measured capacitance (C_p) according to the equation:

$$\varepsilon` = \frac{C_p d}{\varepsilon_o A}$$

where ω is the angular frequency, d is the thickness of the sample (m), ε_o is the permittivity of free space (8.85×10^{-12}), and A is the sample effective surface area (m^2).

2.5. Electrochemical behaviour

Electrochemical investigations will be carried out in a three-electrode conventional glass cell in 1.0 M KOH solution at 25°C using Origalys OGS 200 potentiostat/galvanostat. The potential of the working electrode will be measured against Ag/AgCl reference electrode (E_o = 0.203V vs. SHE) and pure Pt-foil will be used as counter electrode. Cyclic voltammetry curves will be used to characterize the electrochemical behaviour of electrodes at 50 mV s^{-1} potential with sweep rates covering a potential range between -1.4 and 1.0 V (vs. Ag/AgCl) after 5min of immersion in 1.0M KOH (25°C). Cathodic and anodic polarization curves will be measured under a sweep rate of 1.0 mV s^{-1}.

The electrochemical impedance spectroscopy (EIS) of the electrode surface in 1.0 M NaCl at the apparent hydrogen evolution potential has been carried out with an ac voltage amplitude of 10mV using an electrochemical impedance system. The frequency range used in the study was 0.1–10^5 Hz.

3. Result and Discussion

3.1. Characterization

3.1.1. XRD analysis

The XRD patterns for all the samples of Cobalt-Zinc ferrites prepared by microwave combustion and solid state methods are shown in Figures 1 and 2, respectively. The Figures show cubic spinel structure. The peaks at 2θ values of 18.59º, 31.14º, 35.74º, 42.02º, 57.53ºand 62.81º are indexed to (111), (220), (311), (400), (511) and (440) reflections planes of cobalt-zinc ferrites spinel. Some of the miner hematite phase was also observed for P, Co0.2, Co0.5 samples.

Figure 1a-c shows the XRD pattern for $Co_XZn_{1-X}Fe_2O_4$ samples prepared by microwave combustion method and sintered at 800, 1000 and 1400°C. It is observed that the intensities of $Co_XZn_{1-X}Fe_2O_4$ peaks increase up to 1000°C. The hematite contents decreases with increasing the cobalt contents as seen at 800 ºC. Then, almost pure spinel is shown for $Co_{0.8}Zn_{0.2}Fe_2O_4$ sample. In case of the samples sintered at 1000 ºC, the more decrease of hematite is observed for all samples. At 1400ºC, the reformation of hematite is observed beside the spinel phase with decreasing of cobalt contents. This is likely related with the decomposition of cobalt-zinc

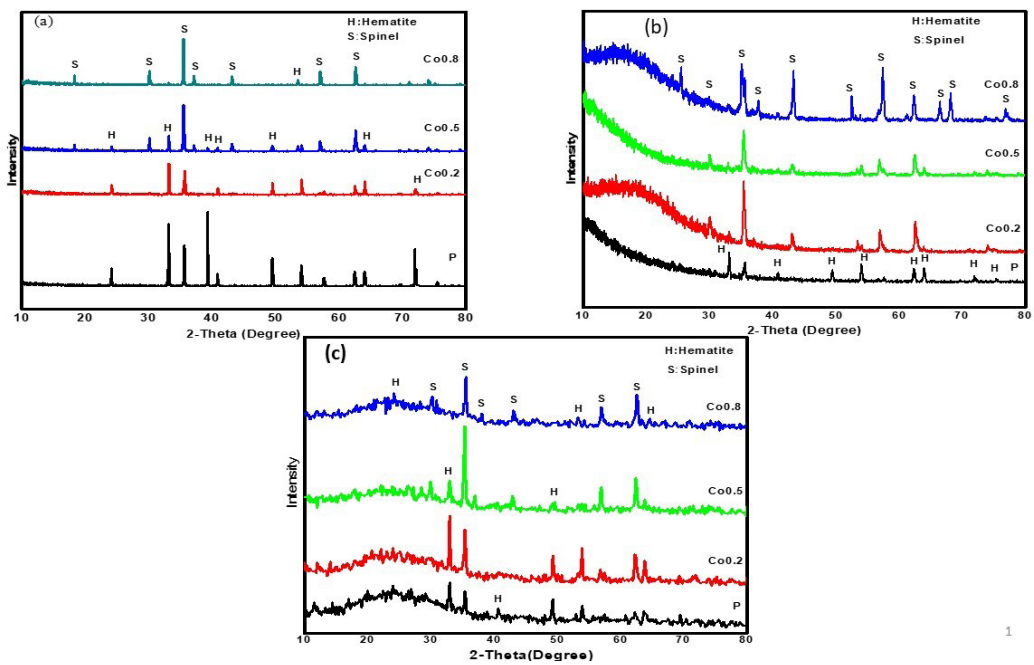

Figure 1. XRD for Cobalt-Zinc ferrites with different Co concentration prepared by microwave method at (a) 800ºC (b) 1000ºC (c) 1400ºC.

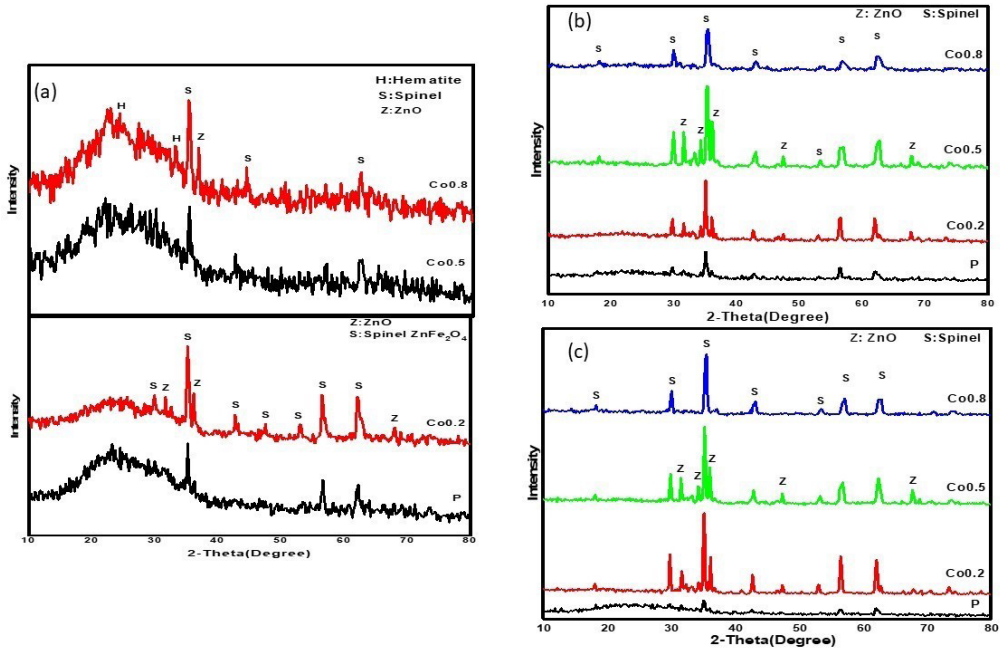

Figure 2. XRD for Cobalt-Zinc ferrites with different Co concentration prepared from EAFD by solid state method at (a) 800ºC (b) 850ºC (c) 900ºC.

ferrite and loss of zinc by evaporation[35] at high temperature. XRD patterns for $Co_XZn_{1-X}Fe_2O_4$ samples prepared by EAFD waste materials at 800, 850 and 900ºC are shown in Figure 2a-c. As seen from Figure 2b, 2c, the intensities of $Co_XZn_{1-X}Fe_2O_4$ increase with increasing the cobalt contents up to 0.5 cobalt content with small traces of hematite and ZnO. After that, the intensity of spinel decreases with smallest amount of other impurity phases ($Co_{0.8}Zn_{0.2}Fe_2O_4$). In addition, the $ZnFe_2O_4$ and $Co_{0.2}Zn_{0.8}Fe_2O_4$ samples show the formation of spinel with some hematite phases. Formation of hematite phase for these samples can be explained as shown previously by decomposition of some spinel at this temperature.

The samples prepared from waste materials indicated that the highest phase of $Co_XZn_{1-X}F_2O_4$ is determined after sintering at 900ºC compared with the samples sintered at 850ºC and 800ºC. In general the sintering of this sample is stopped at 900ºC due to the melting of sample at 1000ºC. This is due to the high CaO content in EAFD waste materials (Table 1). As seen from Figure 2c, the $ZnFe_2O_4$ sample with cobalt shows the formation of mainly spinel phase. In addition, the highest content of spinel structure is obtained for the $Co_{0.2}Zn_{0.8}Fe_2O_4$ combined with some amounts of ZnO. This behaviour is due to larger ionic radius of Zn^{2+} than Co^{2+}, as Zn^{2+} contributes in increasing the lattice parameter[36]. For $Co_{0.8}Zn_{0.2}Fe_2O_4$ sample at 900ºC, the highest purity of this phase is obtained with less amount of ZnO phase. It is also observed that $Co_XZn_{1-X}Fe_2O_4$ spinel phase formation decreases with increasing Co content at 900ºC. This may be explained by the dependence on both ZnO and Fe_2O_3 as extra additions on the EAFD with cobalt oxide to optimize the stoichiometric of $Co_XZn_{1-X}Fe_2O_4$. It was found that increasing cobalt content leads to addition of extra Fe_2O_3 on the expense of ZnO. Fe_2O_3 extra addition leads to enhance the liquid phase formation due to the reaction of some Fe_2O_3 with CaO that retard the spinel formation. Decreasing the intensity of pure $ZnFe_2O_4$ at 900ºC compared with that prepared at 800 ºC may be explained the formation of liquid phase i.e. this batch depended mainly on dust that containing high amount of CaO oxide.

Comparing the XRD pattern in Figures 1a and 2a of the samples fired at 800ºC prepared by the two different methods, It is observed that the diffraction peaks of the samples fired at 800ºC are broader for samples prepared by solid state method based on utilizing EAFD than the prepared by microwave combustion method. In addition the increase of cobalt content enhances the formation of single cubic spinel phase. This behaviour may be due to the difference in the ionic radii between Zn^{+2} (0.74Å) and Co^{+2}(0.65Å)[36]. The microwave enhances the formation of high intensities of spinel structure compared with the solid state method at the same firing temperature. This is behaviour due to the interaction between microwaves and materials via different types of conductions and polarizations losses[37,38], it is believed that microwaves interfacial (grain boundary) polarization and relaxation have contributed significantly to the observed enhanced the grain boundary[36,37].

3.1.2. SEM analysis of $Co_XZn_{1-X}Fe_2O_4$ sintered ceramic samples

SEM is determined for the samples at the optimum selecting temperature. For $Co_XZn_{1-X}Fe_2O_4$ prepared by microwave, 1000ºC is selected to detect the morphology Figure 3. As seen from 0.2 Co containing sample, there are dark gray and light gray particles. The light gray particles are in rounded form with nano sizes that referred to Fe_2O_3 (hematite). The dark gray particles are in prism shapes embedded between the

Fe_2O_3 particles in size ranged from 1-5 µm, that are referred to spinel phase. With increasing the cobalt content, the enhancement of spinel structures is observed.

Figure 4 shows the SEM images of $Co_XZn_{1-X}Fe_2O_4$ samples prepared from EAFD wastes and sintered at 900 °C. It is observed that the sizes of the particles are larger than the samples prepared by microwave. As seen from Figure 4b, the most crowded of the spinel appeared for $Co_{0.2}Zn_{0.8}Fe_2O_4$ samples that grow like agglomerated layer spinel structures with small particles of ZnO. The ZnO particles appear in small white rounded forms. For $Co_{0.8}Zn_{0.2}Fe_2O_4$ image, the well prism forms of spinel structures in larger sizes and the least amounts of ZnO white particle appears in this Figure 4d.

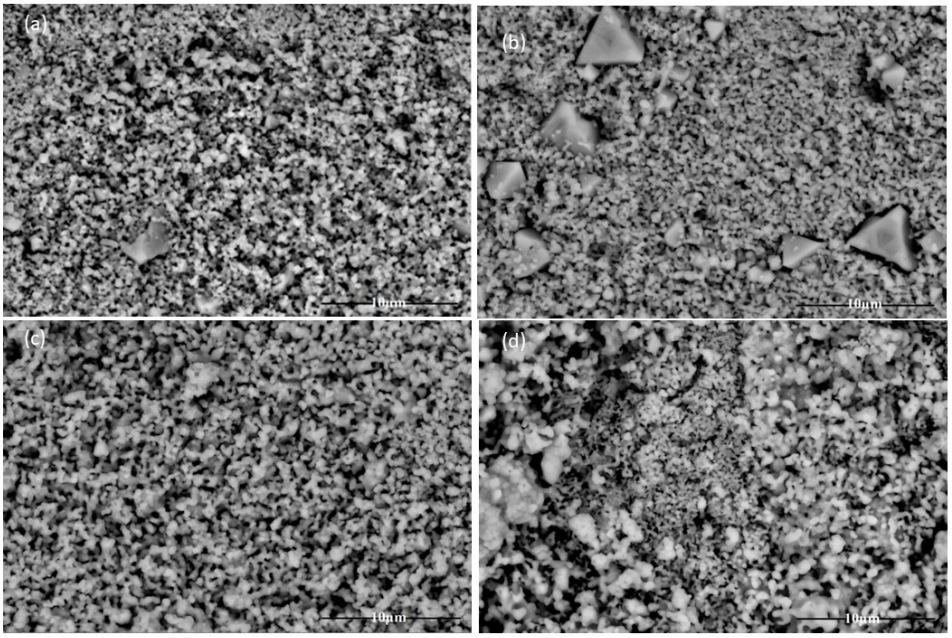

Figure 3. SEM of a) $ZnFe_2O_4$ (b) $Co_{0.2}Zn_{0.8}Fe_2O_4$ (c) $Co_{0.5}Zn_{0.5}Fe_2O_4$ (d) $Co_{0.8}Zn_{0.2}Fe_2O_4$ samples prepared by microwave and sintered at 1000ºC with magnification 12000x.

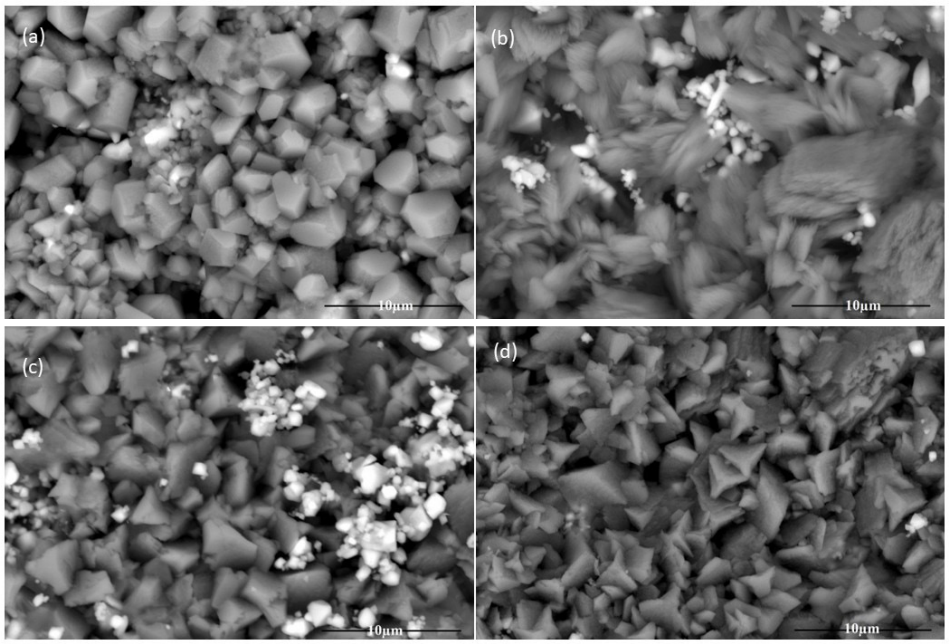

Figure 4. SEM of (a) $ZnFe_2O_4$ (b) $Co_{0.2}Zn_{0.8}Fe_2O_4$ (c) $Co_{0.5}Zn_{0.5}Fe_2O_4$ (d) $Co_{0.8}Zn_{0.2}Fe_2O_4$ samples prepared by solid state method and sintered at 900ºC with magnification 12000x.

3.1.3. Physical properties

The physical properties in term of the bulk density and the apparent density are shown in Figure 5a-d. Physical properties for the samples prepared by Microwave and sintered at 1000 and 1400ºC are shown in Figure 5a, 5b. For solid state method, the physical properties are shown in Figure 5c after firing at 800, 850, 900ºC. It was observed that the bulk density increases and the apparent porosity decreases with increasing the temperature and decreasing in cobalt contents for dust samples. The more decreasing in porosity and increasing in density is observed for microwave samples especially samples sintered at 1400ºC. This behaviour is due to ionic radius of Zn^{2+} is larger than Co^{2+}, as Zn^{2+} contributes in increasing the lattice parameter[39].

3.1.4. Surface area and porous texture analysis of the samples

Nitrogen adsorption-desorption isotherms and Brunauer-Emmett-Teller (BET) equation were used to determine the surface properties and the pore-size distribution of the prepared spinel. As shown from the isotherm in Figures S1 & S2 (supplementary data), the hysteresis loop proves the mesoporous character of the spinel samples which results in good contact with the electrolyte and the enhancement of electrocthemical behavior[40]. The type of isotherm is IV of hysteresis type H4 that confirms the mesoporous properties of the materials and indicates narrow slit- like pores slit-like with inner voids and broad size distribution[41]

The values of the total pore volume V_T, BET surface areas S_{bet}, and the mean pore size are summarized in Table 2. It is noted that the surface area and the pore volume for the samples prepared by solid state method increases with the increase in Co content, however, the sample 0.2Co prepared by microwave method at 1000ºC was the largest one and the high surface area provides more active sites for the HER. The values of the mean pore diameters for all the samples are < 50 nm which indicates mesoporous size.

3.2. Electrical properties of $Co_xZn_{1-x}Fe_2O_4$ ceramic

3.2.1. Electrical properties of $Co_xZn_{1-x}Fe_2O_4$ ceramic prepared by solid state method

Electrical conductivity and dielectric constant studies are very important for materials that are used as electronic devices, sensors and electrocatalyst. Moreover, the frequency and temperature are two essential parameters when studying ac conductivity. Therefore, the dependence of the logarithm of ac electrical conductivity (σ_{ac}) on frequency-temperature for Zn-ferrite ceramic samples with (0.2, 0.5 & 0.8 Co) prepared from dust by solid state method at different sintered temperatures 800, 850 and 900ºC are shown in Figure 6a-c. The ac conductivity increases with increasing frequency, at low frequency, a plateau region in which the conductivity is independent of frequency is obtained and disappeared in some cases. The dispersion of the conductivity with increasing the

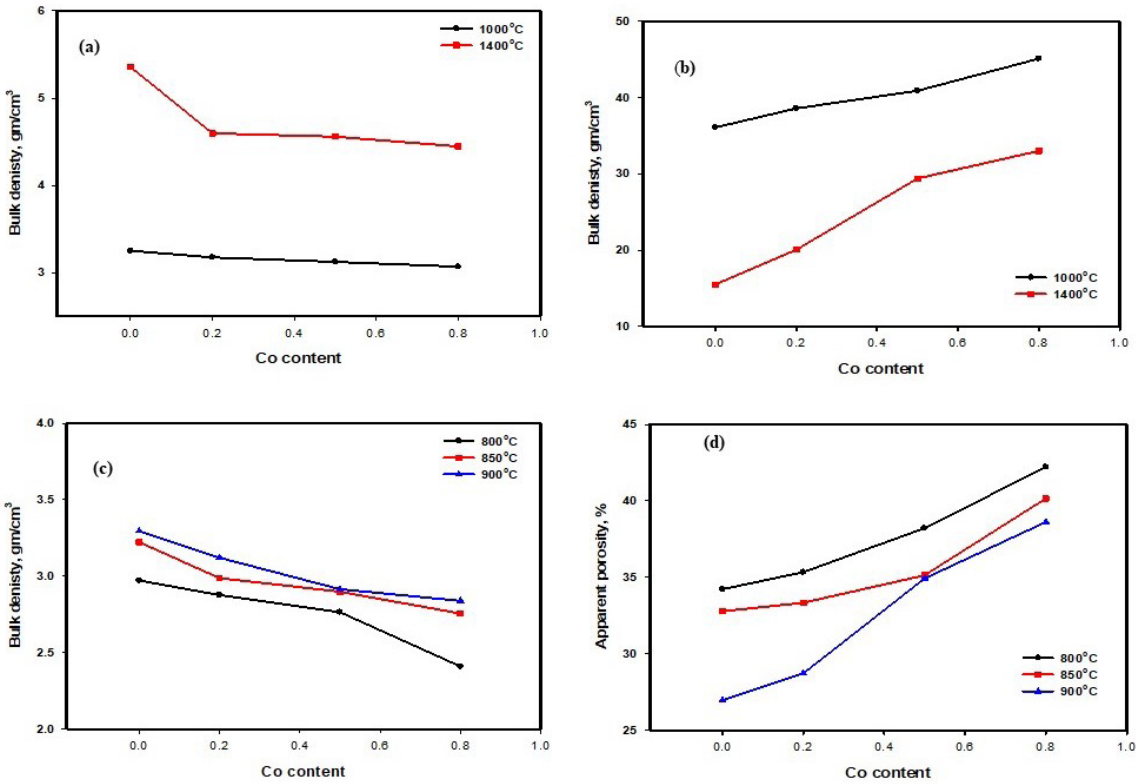

Figure 5. Apparent porosity and bulk density at different temperatures for (a, b) microwave samples and (c, d) for solid state samples.

frequency may be correlate to the jump of ions forward and backward[42]. As shown from Figure 6, ceramic samples with 0.2 and 0.5 Co show the highest conductivity values at low sintered temperature while the sample with 0.8Co shows the highest conductivity values at 900°C. This behaviour is attributed to the decrease in porosity with increasing the sintered temperature and decrease in Co content as discussed in the previous report, and the decrease in porosity results in decreasing the conductivity[43].

The slope of the linear part of the curve at high frequency which represents the frequency exponent s ($0 < s \leq 1$) according to the simple universal power law of Jonscher[44] as given as:

$$\sigma(\omega) = \sigma_{dc} + A\omega^{s}$$

where σ(ω) represents the total conductivity, σ_{dc} is the dc conductivity, A is a constant that depends on the temperature, and ω is the angular frequency. The value of s measures the interaction of the charge carriers with the environment and helps to indicate the mechanism of conduction[45].

Table 2. Porous structure parameters determined by sorption at 77 K for Co-Zinc Ferrite with different Co content prepared by solid state at 800°C and microwave at 1000°C.

Samples	S_{BET} (m^2/g)	V_T (cm^3/g)	Mean pore diameter (nm)
0.2Co/800°C	19.07	0.0759	15.91
0.5Co/800°C	21.07	0.0868	16.47
0.8Co/800°C	29.58	0.1015	13.72
0.2Co/1000 °C/MW	42.85	0.137	12.77
0.5Co/1000 °C/MW	20.46	0.043	7.87
0.8Co/1000 °C/MW	22.07	0.036	6.68

Figure 6d represents the plot of the frequency exponent (s) at different temperatures for the complexes Zn-Ferrite containing 0.2Co, 0.5Co and 0.8Co sintered at different temperature. The values of s are ranging from 0.5 to 1.2. The conduction mechanism has a remarkable relationship with the nature of the plots[46], where the presence of two behaviour indicating two mechanisms for conduction. For Zn-ferrite with 0.2 Co, the s values increase with temperature range from 25-150°C indicating small polaron hopping mechanism while it decreases for temperature higher 150°C which means that it fits the CBH model[45].

The change in the conductivity with the inverse of temperature for the heat treated ceramic samples with (0.2, 0.5 & 0.8 Co) at low frequency (100 Hz) is shown in Figure 6e. The studied conductivity values for Zn-Ferrite containing 0.5, 0.8 Co are linearly dependent on the temperature and increases with increasing temperature, suggesting that the conduction may be due to the hopping of charge carriers. While the conductivity values increase nonlinearly with increasing temperature for sample with 0.2Co, and the curve shows two distinct regions. The different regions indicated different activation energies, which were attributed to different conduction mechanisms. The linear region in the low temperature range can be assigned to electronic conduction, while that in the high temperature region can be attributed to the participation of ions as well as electrons in conduction[47]. From the slope of the linear part, the activation energy ΔE for each sample is calculated according to the following Arrhenius equation:

$$\sigma_T = \sigma_o e^{-\Delta E/KT}$$

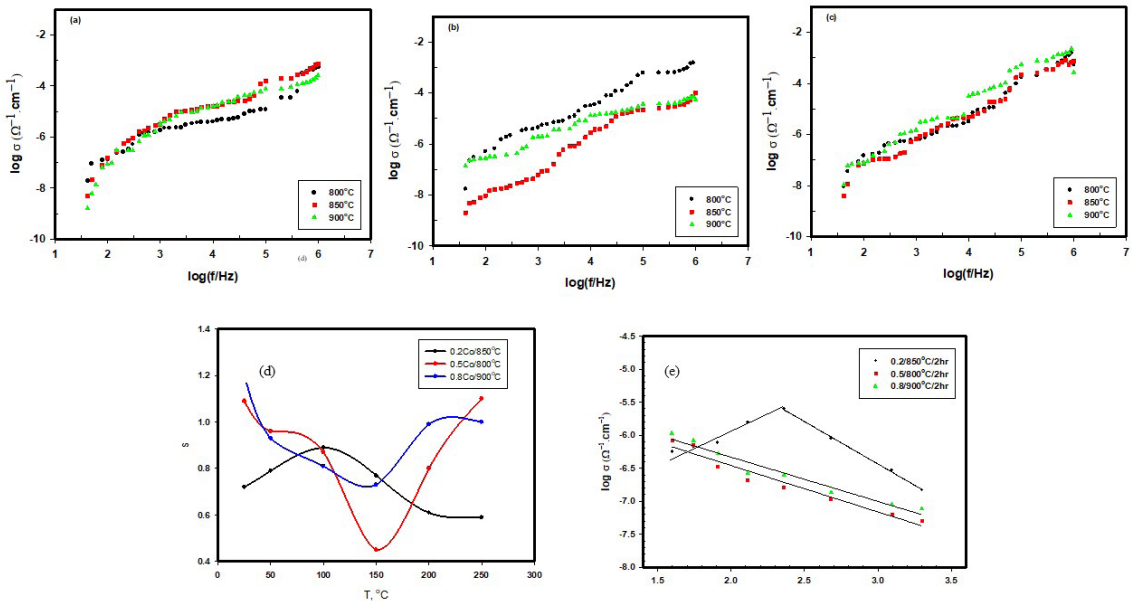

Figure 6. Variation of conductivity with frequency for Zn-ferrite with different concentration of Co ion (a) 0.2, (b) 0.5 (c) 0.8 samples prepared by solid state method and sintered at different temperature (d) The relation between frequency exponent s and the temperature (e) The relation between conductivity and the reciprocal of temperature at 100 Hz.

where σ_T is the conductivity at temperature T(K), σ_o is the pre-exponential factor and K is the Boltzmann constant. The increase in conductivity with increasing temperature indicates that Zn-ferrite doped with Co ions have a positive temperature coefficient and semiconducting properties[48]. This increase in conductivity was attributed to the presence of a d-d* transition in the metal[49].

The values of activation energy for the three samples and the conductivity at low and high frequency are listed in Table 3. The value of the conductivity at low frequencies is in the range of 10^{-7} Ω^{-1}.cm^{-1}, and in the range of 10^{-3} at high frequencies and the low values of Ea (0.013-0.073 eV) suggest that the samples have semiconducting properties[50,51].

The frequency and temperature dependence of the dielectric constant (έ), which was calculated from the measured capacitance for Zn-ferrite with 0.2Co and sintered at 800°C/2hr, is shown in Figure 7a. In general, the normal dielectric behaviour in most ferromagnetic materials was observed where the dielectric constant decreases with increasing frequency of the alternating electric field. This decrease is rapid at low frequencies and becomes slow at high frequencies. At certain frequency depending on Co ion concentration, it becomes independent on frequency. This behaviour was reported previously by Lott et al.[52] which may be due to the interfacial polarization. There is a strong relationship between the dielectric constant values and conduction mechanism[53], the dielectric constant of ferrite depends upon the hopping of electrons between Fe^{2+} and Fe^{3+}, and Co^{2+} and Co^{3+} which results in local movement of electrons that gives high dielectric values. The presence of Co ions forms magnetic cobalt-Ferrite barrier which segregates at grain boundaries results in an increase of Fe^{2+} and decrease of Zn^{2+} inside the grain which leads to an increase in έ. Moreover, different types of defects and dislocations in the crystal lattice encourage the interfacial polarization to be active in low frequency region[54,55].

Table 3. The activation energies (E_a), dc conductivity, capacitance, dielectric constants of the samples prepared by solid state method at room temperature and ac conductivity at 1 MHz and 1 kHz with an experimental error of ±2%.

σ_{ac} ,289K, 1MHz	ε' , 289K, 1KHz	σ_{dc} , 289K	E_a, eV 100 Hz High T	E_a, eV 100 Hz Low T	Sample No.
3.00 x10^{-6}	59.7	1.29x10^{-10}	0.029		**0.2Co/800°C**
1.31 x10^{-5}	1.7	5.15 x10^{-15}	0.026		**0.5Co/800°C**
1.37 x10^{-7}	13.2	1.08 x10^{-11}	0.029		**0.8Co/800°C**
8.79 x10^{-6}	32.4	1.35 x10^{-11}	0.073	0.014	**0.2Co/900°C**
3.78 x10^{-6}	56.9	1.65 x10^{-10}	0.056	0.013	**0.5Co/900°C**
8.33 x10^{-3}	138x10^{4}	3.41x10^{-3}	0.044	0.018	**0.8Co/900°C**

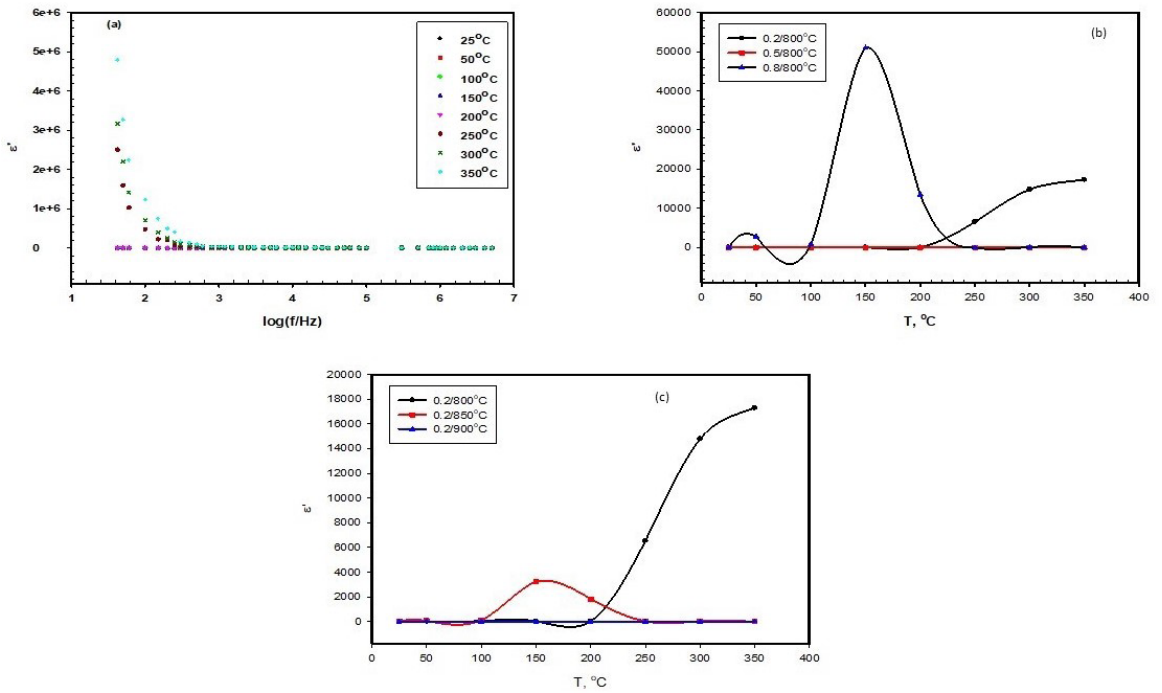

Figure 7. (a) The frequency and temperature dependence of the dielectric constant (έ) for $Co_{0.2}Zn_{0.8}Fe_2O_4$ prepared by solid state and sintered at 800°C/2hr (b) The dependence of dielectric constant on the composition at 10 KHz (c)) The dependence of dielectric constant for $Co_{0.2}Zn_{0.8}Fe_2O_4$ on the sintered temperatures at 10KHz.

According to the recorded data, the dielectric constant is compositional dependent as shown in Figure 7b and the highest values of the dielectric constant (έ) recorded for 0.8Co sintered at 800°C which may be due to the formation of magnetic Ferrite due to the high content of Fe_2O_3 as discussed in XRD section which segregates at the grain boundaries as the concentration of Co^{2+} increases. The dielectric constant is also dependent on the sintered temperature as shown in Figure 7c and the highest values of the dielectric constant (έ) recorded for the samples sintered at 800°C**.**

3.2.2. Electrical properties of $Co_xZn_{1-x}Fe_2O_4$ ceramic prepared by microwave method

The frequency effect on ac electrical conductivity (σ_{ac}) at room temperature for Zn-ferrite ceramic samples which prepared by microwave method at 1000°C are shown in Figure 8a. Independent behaviour of the conductivity on the frequency was shown in low frequencies values followed by an increase with increasing the frequency. The conductivity values increases also with the temperature increase. The frequency dependence of the logarithm of ac electrical conductivity (σ_{ac}) at 300°C for Zn-ferrite ceramic samples with (0.2, 0.5 & 0.8 Co) prepared by microwave method at 1000°C was shown in Figure 8b. The ac conductivity of Zn-ferrite with 0.2Co is higher than the pure Zn-ferrite, as the Co content increases, the conductivity decreases but still higher than the pure sample. This behaviour may be attributed to the formation of hematite beside the spinel phase with decreasing of cobalt contents as mentioned in XRD section.

The dependence of the conductivity on the temperature (in the part of the curve where the conductivity is independent on frequency) for Zn-ferrite ceramic samples with (0.2, 0.5 & 0.8 Co) prepared by microwave method at 1000°C was shown in Figure 8c. The conductivity of the samples increases linearly with increasing the temperature except the sample 0.8Co where the change of conductivity with increasing the temperature shows two linear regions indicating two different conduction mechanisms. The activation energy ΔE for each sample was calculated from the slope of the linear part and was listed in Table 4. The values of activation energy for the samples and the conductivity listed in Table 3. The values of the conductivity at low frequencies are in the range of 10^{-7} $\Omega^{-1}.cm^{-1}$, and in the range of 10^{-2} at high frequencies and low values of E_a suggest semiconducting properties for the samples[47,48].

The frequency-temperature dependence of the dielectric constant (έ) of sample with 0.2Co prepared by microwave method at 1000°C was shown in Figure 9a where a normal dielectric behaviour was observed. The dependence of the dielectric constant (έ) of Zn-ferrite with and without different concentrations of Co on the temperature at 100 Hz was shown in Figure 9b. It was noted that the dielectric constant (έ) decreases with the increase in temperature below 100°C while after that it increases. The values of the dielectric constant (έ) ranges from 25 to 54 which are lower than the values of the samples prepared by solid state that may be due to the decrease of hematite phase in the samples sintered at 1000 °C and as a result there is a decrease in the hopping of electrons between Fe^{2+} and Fe^{3}.

3.3. Electrochemical behaviour

3.3.1. Voltammetric studies

Cyclic voltammetry (CV) technique was used to characterize the prepared materials towards hydrogen evolution in alkaline solution. Figure 10a shows the typical

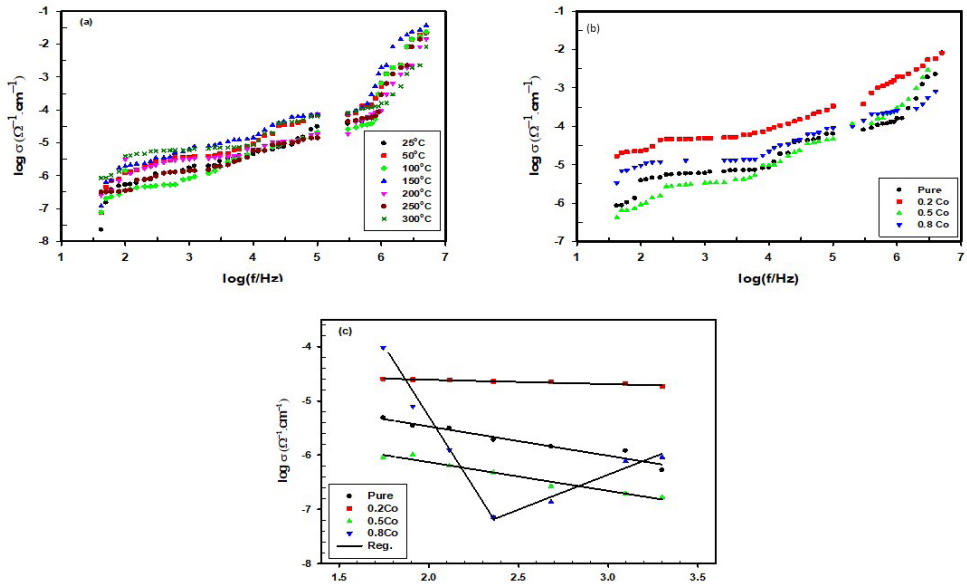

Figure 8. Variation of conductivity with frequency for (a) Zn-ferrite prepared by microwave method at 1000°C (b) for pure Zn-ferrite and Co-Zn-ferrite at at 300°C (c) The relation between the variations of conductivity as a function of the reciprocal of temperature at 100 Hz.

Table 4. Room temperature values of the activation energies (E_a), dc conductivity, capacitance, dielectric constants of the samples prepared by microwave method and sintered at 1000°C and ac conductivity at 1 MHz and 1 kHz with an experimental error of ±2%.

σ_{ac} ,289K, 1MHz	ε' , 289K, 1KHz	σ_{dc} , 289K	E_a, ev 100 Hz High T	E_a, ev 100 Hz Low T	Sample No.
2.0 x10^{-3}	19.5	1.45x10^{-7}	0.029		**0.2Co/1000°C**
8.4 x10^{-4}	13.2	2.67 x10^{-7}	0.019		**0.5Co/1000°C**
4.1 x10^{-5}	6.23	4.20 x10^{-8}	-0.048	0.018	**0.8Co/1000°C**

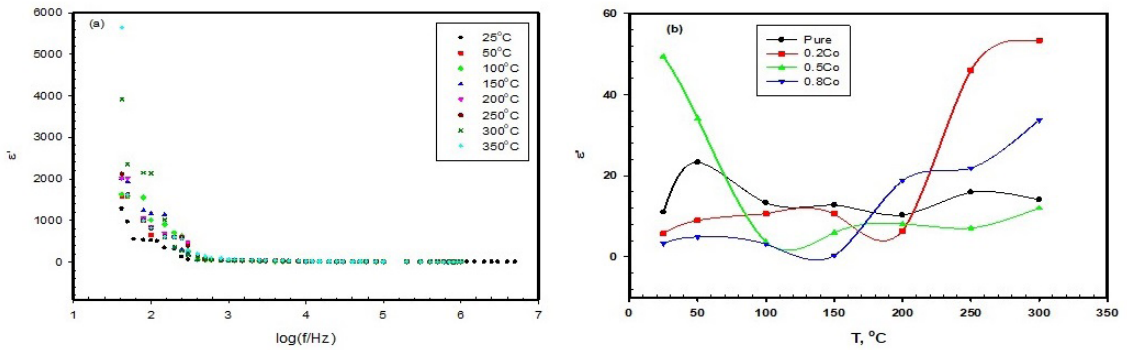

Figure 9. (a) The frequency and temperature dependence of the dielectric constant (έ) for pure Zn-ferrite prepared by microwave method at 1000°C (b) The dependence of dielectric constant on the composition and temperature at 100Hz.

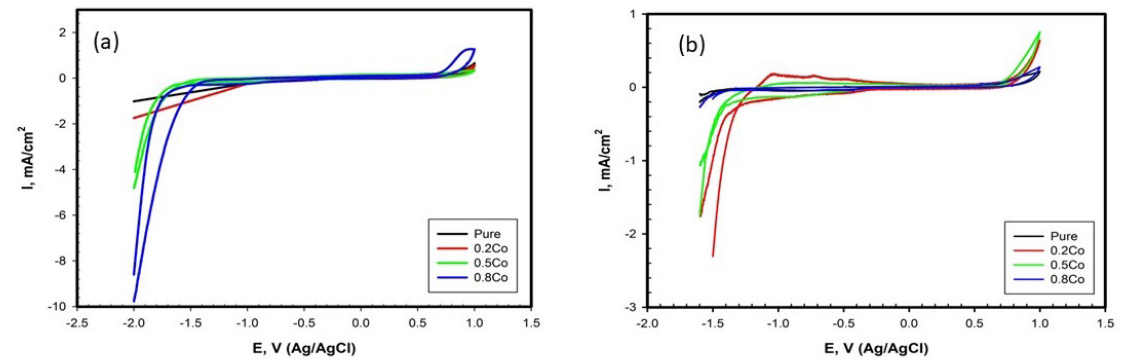

Figure 10. Cyclic voltammetry at scan rate of 50 mV/S in 1.0 M KOH for Zinc Ferrite and Co-Zinc Ferrite prepared by (a) solid state at 800°C (b) microwave at 1000°C.

cyclic voltammograms of Zn-ferrite sample (pure) with different cobalt concentrations (0.2, 0.5 & 0.8) prepared by solid state method at 800°C in the potential range (-1.5-1.0V) at scan rate 50 mV/s. As observed from the voltammgrams, the presence of Co increases the current of both the anodic and cathodic branch. For 0.8Co content, an increase in the cathodic current density due to the hydrogen evolution reaction was observed with the oxide reduction followed by H^+ intercalation and the corresponding anodic current peak due to the de-intercalation process[33]. Also, as the Co content increases in the sample, the potential of the hydrogen evolution shifts to more positive. Thus cyclic voltammetry results demonstrated that the increase in Co content in the ferrite results in good catalytic activity of the ferrite prepared by solid state method for HER reaction.

The typical cyclic voltammograms of ferrite sample (pure) and the cobalt ferrite with different cobalt concentrations (0.2, 0.5 & 0.8) prepared by microwave method at 1000°C in the potential range (-1.5-1.0V) at scan rate 50 mV/s was shown in Figure 10b. The voltamograms look like that corresponding samples prepared by solid state method. However, the values of the anodic and cathodic current densities are larger than in case of the samples prepared by solid state method due to the enhancement in the formation of spinel structure by using microwave. This behaviour suggests the use of $Co_xZn_{1-x}Fe_2O_4$ as anode and cathode electrocatalysis. The first replacement of Zn by 0.2Co ($Co_{0.2}Zn_{0.8}Fe_2O_4$), the cathodic and anodic current density increases then it decreases as the Co content increases but still higher than the pure sample. The change in the elctrocatalytic behaviour of the samples

prepared by solid state and microwave may be due to the variation of phases (zinc oxide or hematite) formed beside the spinel as discussed in XRD section

To systematically study the electrochemical activity of the zinc ferrite and Co-zinc ferrite ceramic samples prepared by solid state method and microwave method, steady state polarization curves were measured in 1.0M KOH at scan rate 1mV/s and shown in Figure 11a, 11b.

The current density of the cathodic branch increased rapidly as the potential increased to more negative values. The initial potential at which hydrogen evolved for the solid state samples (onset potential) for 0.5Co and 0.8Co are -1.37 V and -1.55V respectively. Although the current of hydrogen evolution for 0.8Co sample is larger than 0.5Co, the onset potential of the hydrogen evolution shifts to more negative values as the Co content increases. This may be due to segregates of Fe_2O_3 at the grain boundaries as the concentration of Co^{2+} increases as discussed in XRD section which decreases the electron transfer at the high content Co ferrite sample where spinel with two metal elements would increases the feasibility to tune the energy density and working voltage by varying the metal content[56-58]. However, the increase in Co contents in the microwave samples at 1000°C decreases the current of hydrogen evolution then it increases in case of 0.8Co content but still lower than the base.

In alkaline electrolyte, the hydrogen evolution represented the cathodic-half cell reaction where water transfer to molecular hydrogen and hydroxyl ions ($2H_2O + 2e \leftrightarrow H_2 + 2OH^-$) and the oxygen evolution represented by the anodic-half cell reaction, which is a far more complex process, where the OH^- ions of the cathodic reaction oxidized as the anode to produce oxygen and water molecules ($4OH^- \leftrightarrow O_2 + 2H_2O+4e$). As shown from Figure 10, the prepared samples showed electrocatalyic behaviour for both the cathodic and anodic branch, therefore the anodic electrocatalytic behaviour was also studied for the samples prepared by microwave method at 1000 °C as shown in Figure 11c. A region of OH adsorption on the CoOOH oxyhydroxide was observed at 0.6-1.0V followed by rapid increase in current due to oxygen evolution. As the Co content increases the anodic current density increases and the onset potential of oxygen evolution shifted to low positive values till 0.8Co content where the onset potential increases and the current density decreases.

To quantify the kinetics analysis of the hydrogen evolution reaction, Tafel plots were represented by drawing the over potential versus the logarithm of current density (η vs. log i) as shown in Figure S3a, S3b, and the linear regions of the Tafel plots were fitted into the following Tafel equation:

$$\eta = \frac{2.3RT}{\alpha F} log i_o - \frac{2.3RT}{\alpha F} \log i$$

where η is the overpotential, R is the ideal gas constant (8.314 J/mol.K), i_o is exchange current density, F is the Faraday constant, and T is the absolute temperature. The values of η at 10 mA/cm^2 (η_{10}) for the samples 0.2Co, 0.5Co and 0.8Co prepared by solid state method at 800°C were estimated to be 1.07, 1.01, and 0.4V respectively, and the Tafel slopes (b) were found to be 119, 37.2 and 65 mV/dec for 0.2Co, 0.5Co and 0.8Co, respectively. However η_{10} for 0.2Co, 0.5Co and 0.8Co prepared by microwave method at 1000°C were estimated to be 0.472, 0.496 and 0.522V, respectively and the corresponding Tafel slopes are 42, 76 and 82 mV/dec.

The stability for $Co_{0.8}Zn_{0.2}Fe_2O_4$ prepared by solid state method at 800°C and $Co_{0.2}Zn_{0.8}Fe_2O_4$ prepared by microwave method at 1000°C were tested by continuously cycled for 500 cycles from in 1.0M KOH at a scan rate of 100 mV/s. As shown from Figure 12a, 12b, the current density was

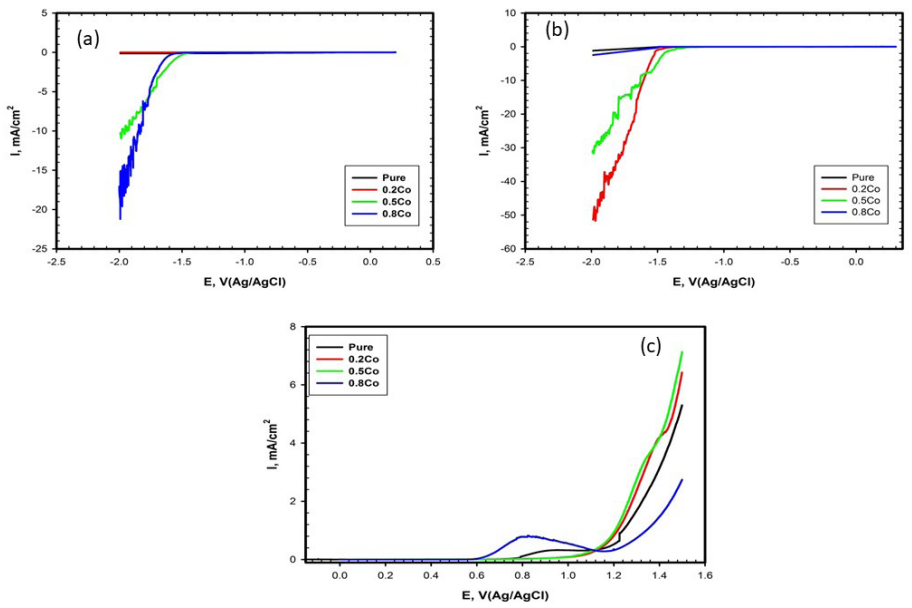

Figure 11. Linear sweep voltammetry at scan rate of 1.0 mV/S in 1.0 M KOH for Zinc Ferrite and Co-Zinc Ferrite prepared by (a) solid state at 800°C (b, c) microwave at 1000°C.

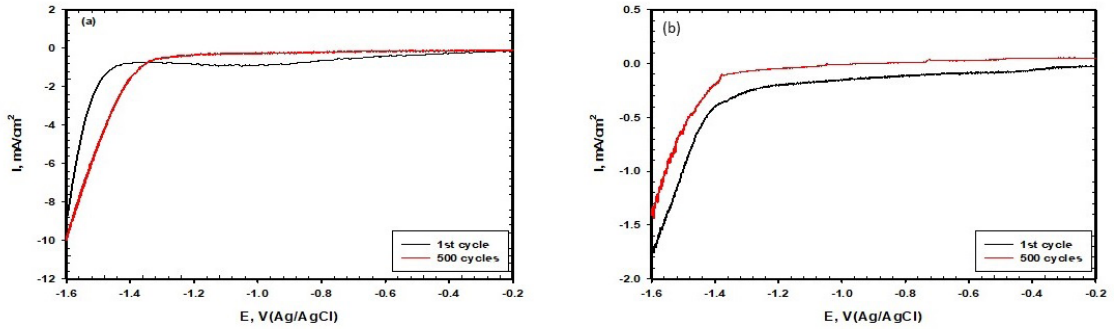

Figure 12. Cyclic stability test for (a) $Co_{0.8}Zn_{0.2}Fe_2O_4$ prepared by solid state method at 800°C and (b) $Co_{0.2}Zn_{0.8}Fe_2O_4$ prepared by microwave method at 1000°C.

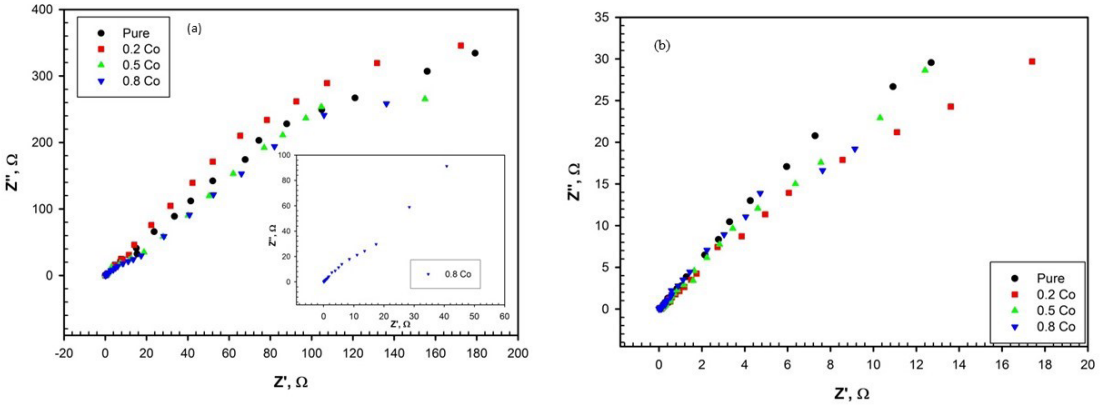

Figure 13. Nyquist plot at potential -1.3 V for Zinc Ferrite and Co-Zinc Ferrite prepared by (a) solid state at 800°C (b) microwave at 1000°C. (Inset: Enlargement of the Nyquist plots in high frequency region).

slightly changed after 500 cycles which may be due to the adsorption of H_2 bubbles on the electrode surface. Both samples show good durability as electrocatalyst for hydrogen evolution in alkaline solution.

EIS was used to investigate the kinetics of the HER reaction. In Figure 13a, the Nyquist plots of the $ZnFe_2O_4$ (pure) and $Co_xZn_{1-x}Fe_2O_4$ with different Co content (0.2, 0.5 and 0.8) prepared by solid state method and sintered at 800°C show a small semicircle at high frequencies representing the sample film, while the large one at intermediate and low frequencies representing with the HER. The diameter of the semicircle at low frequencies for $Co_xZn_{1-x}Fe_2O_4$ is smaller than that of the $ZnFe_2O_4$ (pure) indicating faster charge transfer during HER.

The Nyquist plots of the $ZnFe_2O_4$ (base) and $Co_xZn_{1-x}Fe_2O_4$ with different Co content (0.2, 0.5 and 0.8) prepared by microwave method at 1000°C was shown in Figure 13b, where the behaviour of the samples was the same as the samples prepared by solid state.

4. Acknowledgments

The authors of this work wish to thank the authorities of Science and Technology Development Fund (STDF) for financial support (Research grant No. 25766) to carry out this study.

5. References

1. Mathur P, Thakur A, Lee JH, Singh M. Sustained electromagnetic properties of Ni–Zn–Co nanoferrites for the high-frequency applications. Mater Lett. 2010;64(24):2738-41.
2. Li L, Zhang Y, Li J, Huo W, Li B, Bai J, et al. Facile synthesis of yolk-shell structured $ZnFe_2O_4$ microspheres for enhanced electrocatalytic oxygen evolution reaction. Inorg Chem Front. 2019;6(2):511-20..
3. Majewski P, Krysiå Ski P. Synthesis, surface modifications, and size-sorting of mixed nickel-zinc ferrite colloidal magnetic nanoparticles. Chemistry. 2008;14(26):7961-8.
4. Kaur N, Kaur M. Comparative studies on impact of synthesis methods on structural and magnetic properties of magnesium ferrite nanoparticles. Process Appl Ceram. 2014;8(3):137-43.
5. Valenzuela R. Novel applications of ferrites. Phys Res Int. 2011;2012:591839.
6. Kooti M, Naghdi A. Glycine-assisted fabrication of zinc and manganese ferrite nanoparticle. Sci Iran. 2012;19(2):930-3.
7. Amalthi P, Judith J, Kennedy L, Bououdina M. A Comparative study on the synthesis of Co-doped manganese ferrite [$Mn_{1-x}Co_xFe_2O_4$ (x = 0.0, 0.1, 0.2, 0.3, 0.4, 0.5)] nanoparticles via microwave assisted and conventional combustion method. Chem. Tech. Res. 2014;7:1237-46.

8. Wang Z, Fei W, Qian H, Jin M, Shen H, Jin M, et al. Structure and magnetic properties of $CoFe_2O_4$ ferrites synthesized by sol-gel and microwave calcination. J Sol-Gel Sci Technol. 2012;61(2):289-95.
9. Bhaskar A, Chang TH, Chang HY, Cheng SY. Low-temperature crystallization of sol–gel-derived lead zirconate titanate thin films using 2.45 GHz microwaves. Thin Solid Films. 2007;515(5):2891-6.
10. Sutton WH. Microwave processing of ceramic materials. Am Ceram Soc Bull. 1989;68(2):376-86.
11. Roy R, Agrawal D, Cheng J, Gedevanishvili S. Full sintering of powdered-metal bodies in a microwave field. Nature. 1999;399(6737):668-70.
12. Pigram AJ, Hamlyn MG, Freer R, Bowden AL. Microwave sintering of Ni-Zn ferrites. Ceram Trans. 1993;36:123-31.
13. Sundararajan M, Kennedy LJ, Aruldoss U, Pasha SK, Vijaya JJ, Dunn S. Microwave combustion synthesis of zinc substituted nanocrystalline spinel cobalt ferrite: structural and magnetic studies. Mater Sci Semicond Process. 2015;40:1-10.
14. Khattab RM, Seleman MME-S, Zawrah MF. Assessment of electric arc furnace dust: powder characterization and its sinterability as ceramic product. Ceram Int. 2017;43(15):12939-47.
15. Stathopoulos VN, Papandreou A, Kanellopoulou D, Stournaras CJ. Structural ceramics containing electric arc furnace dust. J Hazard Mater. 2013;262:91-9.
16. Wannakamb S, Manuskijsamrun S, Buggakupta W. The use of electric arc furnace dust from steel recycling in ceramic glaze. Warasan Technol Suranaree. 2013;20(4):329-37.
17. Pelino M, Karamanov A, Pisciella P, Crisucci S, Zonetti D. Vitrification of electric arc furnace dusts. Waste Manag. 2002;22(8):945-9.
18. McCrea J, Pikles CA. Agglomeration and recycling of electric arc furnace dust, *in Electric Furnace Conference Proceedings*, 1995, pp. 351–360.
19. Taha MA, Nassar AH, Zawrah MF. Improvement of wetability, sinterability, mechanical and electrical properties of Al_2O_3-Ni nanocomposites prepared by mechanical alloying. Ceram Int. 2017;43(4):3576-82.
20. Domínguez EA, Ullmann R. Ecological bricks made with clays and steel dust pollutants. Appl Clay Sci. 1996;11(2-4):237-49.
21. Stathopoulos VN, Papandreou A, Kanellopoulou D, Stournaras CJ. Structural ceramics containing electric arc furnace dust. J Hazard Mater. 2013;262:91-9.
22. Vieira CMF, Sanchez R, Monteiro SN, Lalla N, Quaranta N. Recycling of electric arc furnace dust into red ceramic. J Mater Res Technol. 2013;2(2):88-92.
23. Sofilié T, Rastovcan-Mioe A, Cerjan-Stefanovic S, Novosel-Radovic V, Jenko M. Characterization of steel mill electric-arc furnace dust. J Hazard Mater. 2004;109(1-3):59-70.
24. Kulkarani VR, Todhar MM, Vaingankar AS. Electrical Resistivity & Cation Distribution in $Cu_xCd_{1-x}Fe_2O_4$ System. Indian J Pure Appl Phy. 1986;24:294.
25. Rezlescu N, Rezlescu E. Dielectric properties of copper containing ferrites. Phys Status Solidi. 1974;23(2):575-82.
26. Dias A. Microstructural evolution of fast-fired nickel–zinc ferrites from hydrothermal nanopowders. Mater Res Bull. 2000;35(9):1439-46.
27. Mathew DS, Juang RS. An overview of the structure and magnetism of spinel ferrite nanoparticles and their synthesis in microemulsions. Chem Eng J. 2007;129(1-3):51-65.
28. Vestal CR, Zhang ZJ. Synthesis and magnetic characterization of Mn and Co spinel ferrite-silica nanoparticles with tunable magnetic core. Nano Lett. 2003;3(12):1739-43.
29. Fathi AM, Abdel-Hameed SAM, Margha FH, Abdel Ghany NA. Electrocatalytic oxygen evolution on nanoscale crednerite ($CuMnO_2$) composite electrode. Z Phys Chem. 2016;230(10):1519.
30. Guo Y, Zhou X, Tang J, Tanaka S, Kaneti YV, Na J, et al. Multiscale structural optimization: highly efficient hollow iron-doped metal sulfide heterostructures as bifunctional electrocatalysts for water splitting. Nano Energy. 2020;75:104913.
31. Septiani NLW, Kaneti YV, Fathoni KB, Kani K, Allah AE, Yuliarto B, et al.. Self-assembly of two-dimensional bimetallic nickel-cobalt phosphate nanoplates into one-dimensional porous chainlike architecture for efficient oxygen evolution reaction. Chem Mater. 2020;32(16):7005-18.
32. Kaneti YV, Guo Y, Septiani NL, Iqbal M, Jiang X, Takei T, et al. Self-templated fabrication of hierarchical hollow manganese-cobalt phosphide yolk-shell spheres for enhanced oxygen evolution reaction. Chem Eng J. 2021;405:126580.
33. Dymerska A, Kukułka W, Biegun M, Mijowska E. Spinel of nickel-cobalt oxide with rod-like architecture as electrocatalyst for oxygen evolution reaction. Materials. 2020;13(18):3918.
34. Nivetha R, Chella S, Kollu P, Jeong SK, Bhatnagar A, Andrews NG. Cobalt and nickel ferrites based graphene nanocomposites for electrochemical hydrogen evolution. J Magn Magn Mater. 2018;448:165-71.
35. Zhao D-L, Lv Q, Shen Z-M. Fabrication and microwave absorbing properties of Ni–Zn spinel ferrites. J Alloys Compd. 2009;480(2):634-8.
36. Teixeira AMRf, Ogasawara T, Nóbrega MCs. Investigation of sintered cobalt-zinc ferrite synthesized by coprecipitation at different temperatures: a relation between microstructure and hysteresis curves. Mater Res. 2006;9(3):257-62.
37. Sundararajan M, Kennedy LJ, Vijaya JJ, Aruldoss U. Microwave combustion synthesis of $Co_{1-x}Zn_xFe_2O_4$: Structural, magnetic, optical and vibrational spectroscopic studies. Spectrochim Acta A Mol Biomol Spectrosc. 2015;140:421-30.
38. Clark DE, Folz DC, Folgar CE, Mahmoud MM. Microwave solutions for ceramic engineers. Westerville: The American Ceramic Society; 2006.
39. Mahmoud M, Cui Y, Rohde M, Ziebert C, Link G, Seifert H. Microwave crystallization of lithium aluminum germanium phosphate solid-state electrolyte. Materials. 2016;9(7):506.
40. Handal HT, Mohamed WAA, Labib AA, Moustafa SA, Sery AA. The influence of surface modification on the optical and capacitive properties of NiO nanoparticles synthesized via surfactant-assisted coprecipitation. J Energy Storage. 2021;44:103321.
41. Sing KS. Reporting physisorption data for gas/solid systems with special reference to the determination of surface area and porosity. Pure Appl Chem. 1985;57(4):603-19.
42. Choi Y, Baik NI. Preparation of nickel thin sheets with nanosized ferrites by combustion synthesis and electroforming. J Appl Phys. 2011;50(1S2):01BE14.
43. Elliott SR. Ac conduction in amorphous chalcogenide and pnictide semiconductors. Adv Phys. 1987;18:41.
44. Cuevas FG, Montes JM, Cintas J, Urban P. Electrical conductivity and porosity relationship in metal foams. J Porous Mater. 2009;16(6):675-81.
45. Vaish R, Varma KBR. Dielectric properties of $Li_2O–3B_2O_3$-$Li_2O–3B_2O_3$ glasses. J Appl Phys. 2009;106(6):064106.
46. Ebnalwaled AA. Hopping conduction and dielectric properties of InSb bulk crystal. Int J Basic Appl Sci. 2011;11(6):194.
47. Sumi S, Rao PP, Deepa M, Koshy P. Electrical conductivity and impedance spectroscopy studies of cerium based aeschynite type semiconducting oxides: $CeTiMO_6$ (M=Nb or Ta). J Appl Phys. 2010;108(6):063718-9.
48. Mostafaa AG, El-Dosokey AH, Idress KH, Goumaa HM. Study the effect of Mn^{2+} ions on the ac electrical properties of some iron doped phosphate glasses. Int J Res Eng Sci. 2014;2(4):58-63.
49. Bansod AD, Mahale RG, Aswar AS. Synthesis, characterization, electrical and biological studies on some bivalent metal complexes. Rus J Inorg Chem. 2007;52(6):879-83.
50. Linksky JP, Paul TR, Nohre RS, Kenny ME. Studies of a series of haloaluminum, -gallium, and -indium phthalocyanines. Inorg Chem. 1980;19(10):3131-5.

51. Abdel-Hameed SAM, Fathi AM. Preparation and characterization of silver nanoparticles within silicate glass ceramics via modification of ion exchange process. J Alloys Compd. 2010;498(1):71-6.
52. Lott J, Xia C, Kosnosky L, Weder C, Shan J. Terahertz photonic crystals based on barium titanate/polymer nanocomposites. Adv Mater. 2008;20 (19):3649-53.
53. Watawe SC, Sarwade BD, Bellad SS, Sutar BD, Chougule BK. Microstructure, frequency and temperature-dependent dielectric properties of cobalt-substituted lithium ferrites. J Magn Mater. 2000;214(1-2):55-60.
54. Mu G, Chen N, Pan X, Shen H, Gu M. Preparation and microwave absorption properties of barium ferrite nanorods. Mater Lett. 2008;62(6-7):840-2.
55. Kmar BK, Srivastava GP. Dispersion observed in electrical properties of titanium-substituted lithium ferrites. J Appl Phys. 1994;75(10):6115-7.
56. Koo HY, Lee HJ, Go H-A, Lee YB, Bae TS, Kim JK, et al. Graphene-based multifunctional iron oxide nanosheets with tunable properties. Chemistry. 2011;17(4):1214-9.
57. Sun SH, Zeng H, Robinson DB, Raoux S, Rice PM, Wang SX, et al. Monodisperse MFe_2O_4 (M = Fe, Co, Mn) nanoparticles. J Am Chem Soc. 2004;126(1):273-9.
58. Jabeen H, Chandra V, Jung S, Lee JW, Kim KS, Kim SB. Enhanced Cr(VI) removal using iron nanoparticle decorated graphene. Nanoscale. 2011;3(9):3583-95.

Supplementary material

The following online material is available for this article:

Figure S1 – N_2-adsorption/desorption isotherms plots for (a) $Co_{0.2}Zn_{0.8}Fe_2O_4$ (b) $Co_{0.5}Zn_{0.5}Fe_2O_4$ (c) $Co_{0.8}Zn_{0.2}Fe_2O_4$ samples prepared by solid state method and sintered at 800ºC.

Figure S2 – N_2-adsorption/desorption isotherms plots for (a) $Co_{0.2}Zn_{0.8}Fe_2O_4$ (b) $Co_{0.5}Zn_{0.5}Fe_2O_4$ (c) $Co_{0.8}Zn_{0.2}Fe_2O_4$ samples prepared by microwave method and sintered at 1000ºC.

Figure S3 – Tafel plots for $Co_{0.2}Zn_{0.8}Fe_2O_4$, $Co_{0.5}Zn_{0.5}Fe_2O_4$, $Co_{0.8}Zn_{0.2}Fe_2O_4$ samples prepared by (a) solid state method at 800ºC (b) microwave method at 1000ºC.